

Formation of Vacancy Clusters and Electrochemical Control of Electrons in Na_xCoO_2

M.Roger¹, D.J.P. Morris², D.A. Tennant^{3,4}, M.J.Gutmann⁵, J.P. Goff², D.Prabhakaran⁶, N. Shannon⁷, B.Lake⁸, R. Coldea⁶ and P.P. Deen⁹

¹ Orme Merisiers, CEA Saclay, DRECAM, SPEC, F-91191 Gif Sur Yvette, France.

²Department of Physics, University of Liverpool, Oliver Lodge Laboratory, Liverpool L69 7ZE, U.K.

³Hahn-Meitner Institut, Glienicker Str. 100, Berlin D-14109, Germany.

⁴School of Physics and Astronomy, North Haugh, St Andrews, Fife KY16 9SS, U.K.

⁵ISIS Facility, Rutherford Appleton Laboratory, Chilton, Didcot, Oxon OX11 0QX, U.K.

⁶Clarendon Laboratory, Parks Road, Oxford OX1 3PU, U.K.

⁷Univ. Tokyo, Dept Adv Mat Sci, Grad Sch Frontier Sci, 5-1-5 Kashiwahnoha, Chiba 2778851, Japan

⁸Ames Laboratory, Department of Physics and Astronomy, Iowa State University, Ames, IA 50011, U.S.A.

⁹European Synchrotron Radiation Facility, B.P 220, 38043 Grenoble Cedex, France.

In the past decade, high performance batteries based on mobile Li^+ ions in layered metal oxides such as Li_xCoO_2 have made possible a revolution in mobile electronic technology, from iPods to mobile phones¹. Structurally similar Na_xCoO_2 has emerged as a system of fundamental scientific interest because of its highly unusual electrical and magnetic properties. The density, x , of sodium in the intercalation layers can be altered electrochemically, directly changing the number of conduction electrons on metallic CoO_2 sheets². Using neutron diffraction we have detected long-range three-dimensional ordering of Na^+ ions in single crystals of $x=0.78$ and 0.92 and demonstrate a remarkable concentration dependence of Na^+ ordering and vacancy clustering. Large scale numerical simulations show clustering of charged droplets that then order long range. The multivacancy clusters form cages resulting in high thermopower³ for Na_xCoO_2 and their ordering induces a periodic potential in the CoO_2 that readily explains many of the observed electrical and magnetic properties. Electrochemical control of nanoscale devices has great technological potential. Here we show that Na_xCoO_2 provides a model system for exploration.

Within the metallic CoO_2 units, the state of the conduction electrons is unconventional with large effective mass and small Fermi temperature ($\sim 500\text{K}$), a high Seebeck coefficient³, and superconductivity below 5K ⁴ when hydrated. Further, magnetic fields strongly influence the thermopower and it has been proposed that a large spin entropy, associated with the conduction electrons, causes cooling when an electric current flows out (under applied voltage)⁵. Although the exact origin of the transport and magnetic properties is contentious, spin and electronic degrees of freedom of Co ions on the layered hexagonal geometry of CoO_2 are of key importance.

Another remarkable feature of Na_xCoO_2 is that Na^+ ions are able to tunnel between intercalation sites, sandwiched between CoO_2 layers. The Na^+ layers are chargeable electrochemically and measured plateaus and inflections in capacity-voltage⁶ indicate

complex interactions. Recent electron diffraction (ED) measurements reveal Bragg reflections at superlattice positions which alter with concentration, similar to observations in Li_xCoO_2 ⁷. Although the ordering of Li^+ in Li_xCoO_2 has been extensively researched, because of its technological importance, ordering in Na_xCoO_2 has not been considered in detail. Moreover, ED is severely limited because electrons do not penetrate beyond the surface and the scattering is hard to interpret. Neutrons on the other hand penetrate the bulk and provide diffraction data that can be compared with structural models.

We performed neutron diffraction measurements on Na_xCoO_2 single crystals with $x=0.78\pm0.03$ and 0.92 ± 0.03 , see Methods. As well as Bragg reflections from the hexagonal crystal structure (dimensions $a=b=2.84$, $c=10.87\text{\AA}$, $\gamma=120^\circ$, for $x=0.75$) a multitude of much weaker peaks were evident in planes of reciprocal space with a wave-vector transfer perpendicular to the CoO_2 planes of $q_c = 2\pi L/c$ where L is an integer, see Fig. 1. For $x=0.92$, a ring of superlattice peaks form around the main Bragg peaks and the intensity of the rings alternates in L . The superlattice peaks are from long range ordering of Na ions in the bulk and the alternation along L is from the distortion of oxygen positions by nearby Na ions. The peaks are characterised by an incommensurate wave vector in the hexagonal plane of magnitude $\tilde{q} = 0.616 \text{\AA}^{-1}$, and agree with a hexagonal real space unit cell with vectors $\mathbf{a}' = (3\mathbf{a} + \mathbf{b})$ and $\mathbf{b}' = (-\mathbf{a} + 4\mathbf{b})$. The superlattice peaks for $x=0.78$ form a different and very intricate pattern of hexagon-of-hexagons. To understand this diverse and complex behavior we examine the structure more closely.

Sodium ions can occupy sites between oxygen atoms in the CoO_2 layers, as illustrated in Fig. 2. These form two interpenetrating triangular lattices, denoted Na1 and Na2. Cobalt ions lie above and below Na1 sites, resulting in an extra energy cost for occupation relative to an Na2 site. We model this as $\Delta = \Delta_c + \Delta_{sr}$, where Δ_c is a long-range Coulomb contribution and Δ_{sr} a short-range repulsion between Na and Co. Na^+ ions are bigger than the distance between Na1 and Na2 sites, disallowing simultaneous occupancy of nearest neighboring sites making Na ion transport highly nontrivial. For $x>0.8$, Na^+ ions have to pass through gaps between Na^+ ions smaller than their ionic diameter. Classically, this is forbidden. However quantum and thermal fluctuations permit the Na ions to diffuse, and so form ordered states. At lower concentrations the ions interact mainly through a Coulomb repulsion which is partially screened by the electrons in the CoO_2 layers.

Previous theoretical investigations^{8,9} utilise first-principles calculations limited to zero temperature and small cluster sizes. We adopt a radically different approach and consider a Na model retaining only three essential ingredients: long-range Coulomb potential $e^2/(4\pi\epsilon\epsilon_0 r)$ (the dielectric constant ϵ taken as isotropic), short range Na-Na ion shell repulsion V between the neighbours on the same sublattice, and the onsite energy gap Δ . (Elastic deformations of the lattice are neglected). Monte Carlo simulations are then undertaken for realistic sized clusters as outlined in Methods.

Our simulations reveal that the spontaneous formation of multivacancy clusters drives the organization of sodiums, as illustrated in Fig. 2. Vacancies become attractive at very short length scales, through a delicate balance of Coulomb forces and onsite Na1 energy, and condense into droplets. As droplet size increases, the extra energy cost of Na1 sites in the droplet core eventually cancels the energy gain of the droplet surface.

Such droplets are thermodynamically stable only below a characteristic temperature T_C . Droplet ordering gives rise to an anomaly in the internal energy and heat capacity, which is shown in the inset of Fig. 3. The mean spacing between vacancies is determined by the concentration of sodium ions in the material and the formation of different sized droplets depends subtly on the space filling constraints and cooperative ordering of different geometries of clusters.

Monte-Carlo results at room temperature are presented in Fig. 3. The sodium concentration versus chemical potential is characterized by plateaus roughly comparable to those appearing in electrochemical cells⁶. These correspond to stable sodium superstructures at fractional occupancies $x=1/4$, $1/3$, $1/2$, $5/7$, and $3/4$. The $1/4$ and $1/3$ fillings have all sodiums on Na_2 sites, and a simple commensurate triangular structure with real-space unit-cell vectors $\{\mathbf{a}'=2\mathbf{a}; \mathbf{b}'=2\mathbf{b}\}$ and $\{\mathbf{a}'=2\mathbf{a}-\mathbf{b}; \mathbf{b}'=\mathbf{a}+\mathbf{b}\}$ respectively. At higher occupations Na_1 and Na_2 sublattices show strong interplay, in excellent agreement with recent neutron diffraction¹⁰. The $1/2$ -structure forms an $\mathbf{a}'=2\mathbf{a}$ and $\mathbf{b}'=\mathbf{a}+2\mathbf{b}$ ordered structure with equal occupation of Na_1 and Na_2 sites, giving reciprocal lattice vectors in perfect agreement with the ED measurements from $\text{Na}_{0.5}\text{CoO}_2$ ¹¹. The calculated contribution to the heat capacity for $x=1/2$ from Na ordering shows a sharp peak at $T \approx 450\text{K}$ consistent with the disappearance of the superstructure peaks¹² in the ED pattern above ~ 470 K. The $x=5/7$ structure forms an array of divacancy clusters and has unit cell vectors $\mathbf{a}'=3\mathbf{a}-\mathbf{b}$ and $\mathbf{b}'=\mathbf{a}+2\mathbf{b}$. In contrast $x=3/4$ forms an array of trivacancies with supercell unit vectors $\mathbf{a}'=2\mathbf{a}+2\mathbf{b}$ and $\mathbf{b}'=\mathbf{a}+2\mathbf{b}$.

The pair correlation functions measured in diffraction experiments may be obtained from the computed configurations. For $x=5/7$ and $x=3/4$ similar diffraction patterns to those from ED for $x=0.64$ ¹³ and 0.75 ¹⁴ are obtained. However, detailed comparison with ED is not possible since the composition of the surface differs from the bulk and the observed patterns vary over the sample and with exposure to the electron beam¹³. Random mixing of di-, tri- and quadri-vacancies occurs for $x=0.87$ with sharp superstructure reflections at similar wave-vectors to those found for our $x=0.92$ sample in Fig. 1. In order to reproduce the modulation of the scattering along L , the distortion of oxygen atoms next to a divacancy shown in Fig. 1e is required. Figures 1b and d show the scattering calculated with a divacancy cluster model with in-plane unit cell vectors $\mathbf{a}'=3\mathbf{a}+\mathbf{b}$ and $\mathbf{b}'=-\mathbf{a}+4\mathbf{b}$, and divacancies in successive Na planes stacked immediately above each other. This minimal model successfully reproduces the scattering in Figs 1a and c.

Between plateaus rich and complex behaviour arises and self-similar fractal-like structures for Na ordering appear. Indeed the data at $x=0.78$ shows a particularly intricate diffraction pattern displaying a superlattice of hexagon-of-hexagons, see Figs 1f and g. For this concentration small perturbations are expected to lead to complicated ordering patterns. The wave vector of the superlattice is small implying a very large unit cell, and modeling the structure is a challenging crystallographic problem.

The concentration controls the sodium patterning whose electrostatic potential in turn determines the electronic state in the Co layers, as illustrated in Fig. 4. The depth of electrostatic potential wells, $\sim 100\text{meV}$, is larger than the single-particle hopping frequency $t \sim 10 \text{ meV}^{15}$ and so will localize holes. While total energy differences are insignificant ($\sim 0.1\text{meV}$), the Coulomb landscape varies drastically in terms of relative

position of vacancy clusters in successive layers and the ordering along c will be fixed by elastic deformations and coupling between sodium and cobalt charges.

At $x=1/2$ there are only two configurations, with vacancies displaced by **b** (Fig. 4a), and aligned (Fig. 4b). The displaced configuration has one-dimensional character with high and low Coulomb-potential stripes in agreement with the low and high spin charge-ordered stripes found using neutron diffraction¹⁶. Two-hole exchange along the stripes of high spin will be dominant, and this leads naturally to the observed antiferromagnetic structure. A large magnetic field, parallel to the (**a**, **b**) plane favors alignment of holes (divacancies) in c -direction corresponding to Fig. 4b with 2D character. This explains the abrupt change from an insulating antiferromagnet to a conducting state with reconstruction of a 2D Fermi surface above 40T¹⁷.

For $x=5/7$ we expect two holes per potential well. One should occupy the Co site at the well minimum and the second the remaining six Co sites on the potential contour 60meV higher in energy. This configuration is consistent with the 19±4% of Co^{3.7+} observed through NMR¹⁸ which then correspond to the 1/7 of Co sites sitting at potential minima, the remaining sites being Co^{3.3+} and Co³⁺. At low temperature, the two holes may pair into a nonmagnetic singlet state, thus explaining the absence of magnetism at concentration $x\sim 0.7$.

The $x=3/4$ phase, Fig. 4d gives potential wells which sit on a triangular lattice with unit vectors $\mathbf{a}''=2\mathbf{a}$ and $\mathbf{b}''=2\mathbf{b}$, with one hole per well. The hopping frequency among the four sites in a well is expected to be larger than for hopping between sites in different wells. Ferromagnetic ring exchange of three holes in neighbouring wells could account for the observed ferromagnetic sheets¹⁹. Magnetic excitations reveal 3D magnetism²⁰ which can be explained by the fact that the spacing between the moments “trapped” by the potential of trivacancies in-plane is comparable to that between the planes.

Notably di- and tri-vacancy clusters form cages in which Na ions can vibrate relatively freely. These would be expected to disrupt the propagation of phonon excitations, leading to a low thermal conductivity. This behaviour is confirmed in the low temperature-independent thermal conductivity reported¹¹ for metallic Na_xCoO₂. The rare coincidence of high electrical conductivity and low thermal conductivity are precisely the conditions required for the observed high thermopower.

Finally in the superconducting bi-hydrate (Na_xCoO₂·yH₂O) water molecules are intercalated *between* the Na⁺ ions and the CoO₂ planes, and screen electrons participating in superconductivity from the Na⁺ ordering potential. We anticipate that the electrochemical control of electronic states in Na_xCoO₂ through Na⁺ ion ordering will be extremely sensitive to the intercalation of water. The failure of the mono-hydrates - in which water molecules are intercalated *within* the planes of Na⁺ ions - to superconduct²¹, reinforces this point of view.

In summary, complex orderings of multi-vacancy clusters have been discovered using neutron diffraction and successfully modelled by taking into account the various coulomb interactions. The resulting periodic electrostatic potential in the Co planes has important implications for the thermoelectric, magnetic, and superconducting properties of Na_xCoO₂. The well defined ordering of the sodium subsystem makes this a model material to explore electrochemical control of magnetism, and electrical and thermal transport properties.

Methods

Neutron diffraction

Neutron Laue diffraction provides a powerful technique with which to probe atomic ordering in the bulk of a crystal sample. Single crystal data were collected on the SXD diffractometer at the ISIS pulsed neutron source, Rutherford Appleton Laboratory, UK. SXD combines the white beam Laue technique with area detectors covering a solid-angle of 2π steradians allowing comprehensive data sets to be collected. Measurements were made from samples obtained from zone-melted rods of $\text{Na}_{0.78}\text{CoO}_2$ and $\text{Na}_{0.92}\text{CoO}_2$ grown using the floating zone method²². Single crystals from the rods were initially screened and a suitable piece in each case cut away. This was mounted at the end of an aluminium pin and cooled to 150 K using a closed-cycle He refrigerator. Four and five orientations were collected for the $x=0.78$ and $x=0.92$ crystals for 35 and 11 hours per orientation respectively. Data were corrected for incident flux using a null-scattering V/Nb sphere. These data were then combined to a volume in reciprocal space and sliced to obtain individual planar cuts. Other small samples from the same rods were examined by x-ray diffraction and magnetometry to determine their quality and EPMA their composition (to $\sim 3\%$). Small inclusions of a few percent of the cobalt oxides (CoO and Co_3O_4) as well as Na_2O were found. The diffraction measurements show that these grow epitaxially on the host lattice and the impurity signal is straightforward to distinguish from that from the Na_xCoO_2 .

Monte Carlo calculations

Monte-Carlo simulations were performed within the Grand-Canonical ensemble using the method described by Adams²³. In this, the chemical potential is fixed and the mean number $\langle x \rangle$ of sodium ions at equilibrium determined within the simulation. More precisely, the relevant quantity is $\langle x \rangle$ as a function of μ^{ex} , the excess of the chemical potential relative to that of an ideal gas²³. We simulate two Na layers, each containing a maximum number of 1176 ions embedded in an orthorhombic crystal of size $42a \times 28a\sqrt{3} \times c$ with periodic boundary conditions in the three dimensions. The unit cell parameters are those measured in the $x=0.75$ phase: $a=2.84\text{\AA}$ and $c=10.87\text{\AA}$ ¹⁰. The long-range Coulomb interactions are summed through a variant of the Ewald procedure. The number of sodium ions is varied at neutral global charge. The following types of updating are attempted: (1) adding simultaneously a Na^+ ion and a negative charge in the Co planes; and with the same probability: (2) removing a Na^+ ion and adding a positive charge in the Co planes; (3) moving Na^+ ions at constant particle number: we permit nearest neighbor as well as long-range displacements of individual ions and also global movements of vacancy clusters. The simulations start with $x=0$, i.e. a CoO_2 crystal with no sodium and all cobalt ions in a Co^{4+} state. Each time a sodium on a Na1 or Na2 site is added a negative charge is added in the Co layers: i.e a Co^{4+} is changed to a Co^{3+} . Although the effective mass of electrons (or holes) in the Co layers can reach 50 times the mass of a free electron, it is still two orders of magnitude lower than the mass of the sodium ions so at time-scales relative to the sodium ions we consider all screening charges to be uniformly spread out on the cobalt sites. This approximation is sufficient for the study of in-plane sodium ordering, which will be the dominant ingredient in the

formation of superstructures. It will be relaxed in future studies to account for cooperative Na-Co charge-ordering phenomena in the third dimension.

Acknowledgements

We wish to thank Steve Lee and John Irvine of St Andrews University, Paolo Radaelli of Rutherford Appleton Laboratory, Trahn Trung Nguyen of CEA, Saclay, Andrew Boothroyd of the Clarendon Laboratory and Minoru Nohara of Tokyo University for helpful discussions, and Themis Bowcock and Andrew Washbrook for the use of the MAP2 supercomputer at the University of Liverpool.

Competing interest statement

The authors declare that they have no competing financial interests.

Correspondence and requests for materials should be addressed to M.R. (e-mail: roger@drecam.saclay.cea.fr).

References

1. Tarascon, J.-M. and Armand M. Issues and challenges facing rechargeable lithium batteries. *Nature* **414** 359-367 (2001).
2. Delmas, C., *et al.* Electrochemical intercalation of sodium in Na_xCoO_2 bronzes. *Solid State Ionics* **3-4** 165-169 (1981).
3. Terasaki, I., Sasago, Y. & Uchinokura, K. Large thermoelectric power in NaCo_2O_4 single crystals. *Phys. Rev. B* **56**, R12685- R12687 (1997).
4. Takada, K., *et al.* Superconductivity in two-dimensional CoO_2 layers. *Nature* **422**, 53-55 (2003).
5. Wang, Y.Y., Rogado, N.S., Cava, R.J. & Ong, N.P. Spin entropy as the likely source of enhanced thermopower in $\text{Na}_x\text{Co}_2\text{O}_4$. *Nature* **423**, 425-428 (2003).
6. Amatucci, G. G., Tarascon, J. M. & Klein, L. C. CoO_2 , The End Member of the Li_xCoO_2 Solid Solution. *J. Electrochem. Soc.* **143**, 1114-1123 (1996).
7. Shao-Horn, Y., *et al.* Li and vacancy ordering in $\text{T}^{\#2}\text{-Li}_x\text{CoO}_2$ derived from O_2 -type LiCoO_2 . *Chem. Mater.* **15** 2977-2983 (2003).
8. Arroyo y de Dompablo, M. E., Van der Ven, A. & Ceder, G. First-principles calculations of lithium ordering and phase stability on Li_xNiO_2 . *Phys. Rev. B* **66**, 064112 1-9 (2002).
9. Zhang, P., Capaz, R. B., Cohen, M. L. & Louie, S. G. Theory of sodium ordering in Na_xCoO_2 . *Phys. Rev. B* **71**, 153102 (2005).
10. Huang, Q., *et al.* Low temperature phase transition and crystal structure of $\text{Na}_{0.5}\text{CoO}_2$. *J. of Phys. Cond. Mat.* **16**, 5803-14 (2004).
11. Foo, M. L., *et al.* Charge Ordering, Commensurability, and Metallicity in the Phase Diagram of the Layered Na_xCoO_2 *Phys. Rev. Lett.* **92**, 247001 (2004).
12. Yang, H. X., *et al.* Structural phase transitions and sodium ordering in $\text{Na}_{0.5}\text{CoO}_2$: a combined Electron diffraction and Raman Spectroscopy study. *Solid State Comm.* **134** (6): 403-408 (2005).
13. Zandbergen, H. W. *et al.* Sodium ion ordering in Na_xCoO_2 : Electron diffraction study. *Phys. Rev. B* **70** 024101 (2004).

14. Shi, Y. G., *et al.*, Superstructure, sodium ordering and antiferromagnetism in Na_xCoO_2 ($0.75 \leq x \leq 1.0$). <http://arxiv.org/cond-mat/0401052> (2004).
15. Hasan, M. Z., *et al.* Fermi surface and quasiparticle dynamics of $\text{Na}_{0.7}\text{CoO}_2$ investigated by angle-resolved photoemission spectroscopy. *Phys. Rev. Lett.* **92**, 246402/1-4 (2004).
16. Yokoi, M. *et al.*, Magnetic Correlation of Na_xCoO_2 and Successive Phase Transitions of $\text{Na}_{0.5}\text{CoO}_2$ – NMR and Neutron Diffraction Studies, <http://arxiv.org/cond-mat/0506220> (2005).
17. Balicas L. *et al.* Shubnikov-de Haas oscillations and the magnetic field induced suppression of the charge ordered state in $\text{Na}_{0.5}\text{CoO}_2$, *Phys. Rev. Lett.* **94**, 236402 1-4 (2005).
18. Mukhamedshin, I. R., Alloul, H., Collin, G. & Blanchard, N. ^{59}Co NMR study of the Co states in superconducting and anhydrous cobaltates. *Phys. Rev. Lett.* **94**, 247602 (2005).
19. Bayrakci, S. P., *et al.* Magnetic Ordering and Spin Waves in $\text{Na}_{0.82}\text{CoO}_2$. *Phys. Rev. Lett.* **94**, 157205 (2005).
20. Helme, L. M., *et al.* Three-Dimensional Spin Fluctuations in $\text{Na}_{0.75}\text{CoO}_2$. *Phys. Rev. Lett.* **94**, 157206 (2005).
21. Sakurai, H., Takada, K., Izumi, F., Dilanian, R.A., Sasaki, T. & Takayama-Muromachi, E. The role of the water molecules in novel superconductor, $\text{Na}_{0.35}\text{CoO}_2 \cdot 1.3\text{H}_2\text{O}$, *Physica C: Superconductivity*, **412-414**, 182-186 (2004).
22. Prabhakaran, D., Boothroyd, A. T., Coldea, R. & Charnley, N. R. Crystal growth of Na_xCoO_2 under different atmospheres. *J. Crystal Growth* **271**, 74-80 (2004).
23. Adams, D. J. Grand canonical ensemble Monte Carlo for a Lennard-Jones fluid. *Mol. Phys.* **29**, 307-311 (1975).
24. Chou, F. C., *et al.* Thermodynamic and Transport Measurements of Superconducting $\text{Na}_{0.3}\text{CoO}_2 \cdot 1.3\text{H}_2\text{O}$ Single Crystals Prepared by Electrochemical Deintercalation. *Phys. Rev. Lett.* **92**, 157004 (2004).
25. Klein, M. & McDonald, I. R. Properties of the paraelectric-solid and molten phases of sodium nitrite. *Proc. Roy. Soc. Lond. A* **382**, 471-482 (1982).

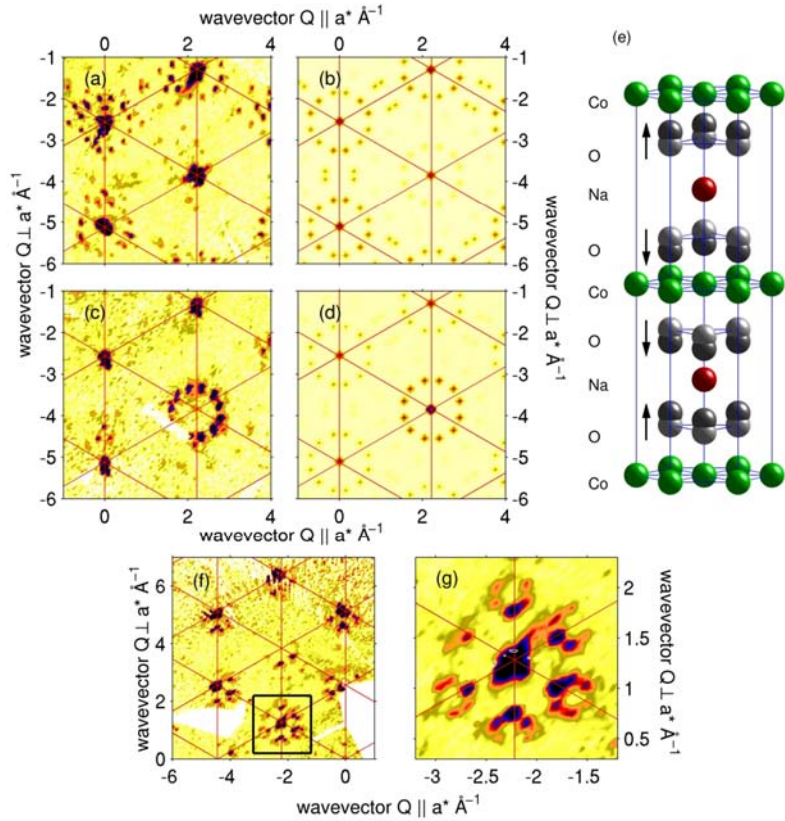


Figure 1. Neutron diffraction showing bulk 3D ordering of Na^+ . (a) $(H, K, 6)$ plane for $x=0.92$, superlattice reflections form rings around hexagonal Bragg reflections. (b) Calculated scattering from divacancy clusters arrayed on superstructure with real space vectors $\mathbf{a}'=3\mathbf{a}+\mathbf{b}$, $\mathbf{b}'=-\mathbf{a}+4\mathbf{b}$. The lattice is averaged over all domains; typically only a single domain would be observed using electron diffraction. (c) Relative intensities of scattering around hexagonal Bragg peaks change with L ; $(H, K, 11)$ shows opposite trend to $(H, K, 6)$ plane in (a). (d) Calculated scattering captures observed modulation along L when oxygen ions next to divacancy clusters are distorted, see (e). (f) For $x=0.78$ in the $(H, K, 7)$ plane larger cell reflections are observed and, on an expanded scale (g) hexagon-of-hexagons.

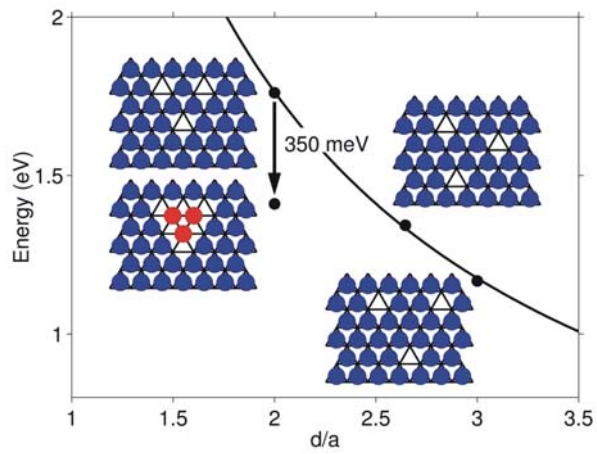
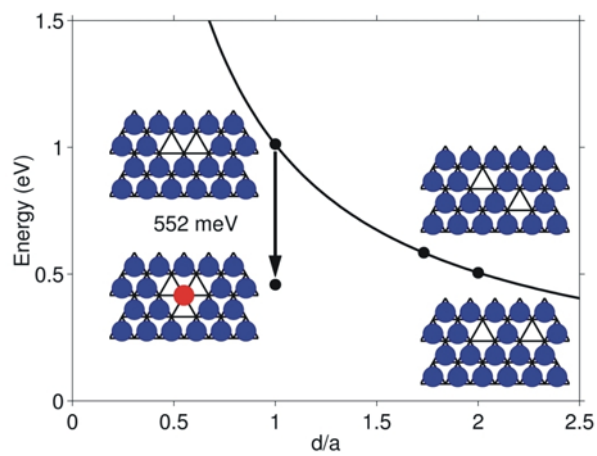
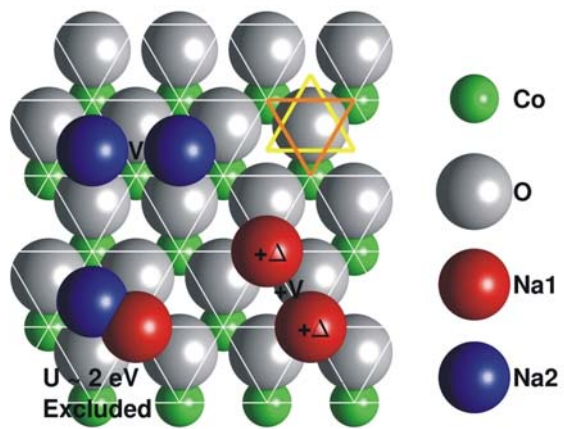


Figure (2): Na_xCoO_2 has Na^+ ions intercalated between CoO_2 layers. (top) Two interpenetrating hexagonal lattices of intercalation sites denoted Na1 , and Na2 in a repeated Star-of-David motif (yellow)¹ are formed. Ions are shown to scale. (middle) Energy for two vacancies is inversely proportional to distance as expected for Coulomb repulsion. Neighbouring vacancies can reduce their energy by promotion of a Na2 sodium to the central Na1 site. The resultant *divacancy* cluster has net charge $2e^-$ spread over three sites and substantially lower energy as central sodium is now further from its neighbors. Its stabilization energy is lower than vacancies 3-4 sites apart so should form spontaneously at modest concentrations. (bottom) Formation of a trivacancy follows a similar process and three vacancies combine with $\text{Na2} \rightarrow \text{Na1}$ promotions. The extra 3Δ energy penalty makes a trivacancy have a lower stabilization energy than a divacancy and has a charge $3e^-$ spread over 6 sites.

¹ The minimal model for the sodium system can be mapped onto an Ising model where a spin state $S_i^z = +1/2$ denotes that the i th site of the honeycomb lattice is occupied, and $S_i^z = -1/2$ that it is empty. The electrostatic and ionic shell interactions are represented by the Hamiltonian:

$$H = \sum_{ij} (V_{ij} + cr_{ij}) (\sigma_i^z + 1/2) (\sigma_j^z + 1/2) + \sum_i (-\mu + \Delta(1 + (-1)^i)) (\sigma_i^z + 1/2),$$

where only shell repulsions V_{ij} for nearest neighbor (U) and next-nearest neighbor interactions (V) are treated as important, c absorbs the Coulomb repulsions, and the chemical potential μ acts as a uniform field, and Na1 onsite energy Δ like a staggered field. Such models on frustrated lattices are known to be highly degenerate and to show plateau behaviour with field. Critical behaviour can also arise.

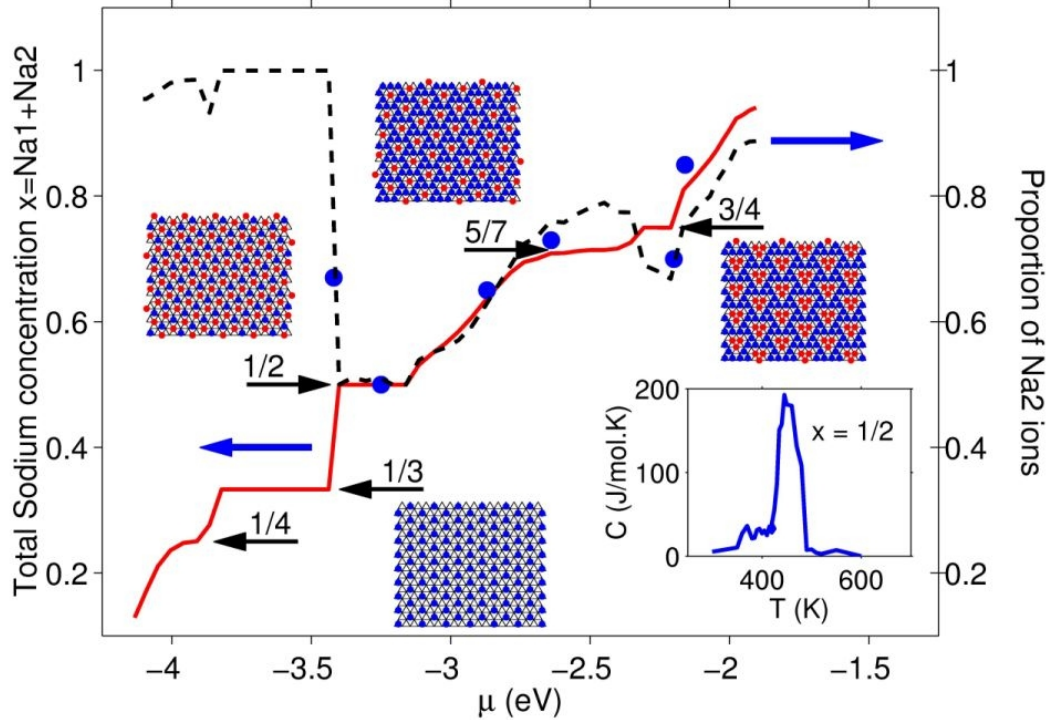


Figure 3: Variation of sodium density versus chemical potential - solid line. A choice of $\varepsilon = 6$ gives an increase in chemical potential of 1.2 eV between $x=0.2$ and 0.6, in agreement with observed changes in voltage in electrochemical cells with dry electrolyte⁶. More recent voltage versus capacity curves obtained using NaOH as solvent²⁴ show smaller voltage variations, comparable to $\varepsilon = 16$, however this higher value is consistent with the fact that $(\text{H}_3\text{O})^+$ oxonium ions penetrate the structure, screening the Coulomb interaction. The influence of V and Δ is strongest at the highest concentrations, altering the range of stability of the ordered phases. We use the values $V=0.04$ eV and $\Delta_{sr} = 0.01$ eV, which are within the range compatible with available data for short-range Na-Na and Na-Co ion shell repulsions in various salts²⁵. The dashed line is the calculated proportion of sodiuns occupying Na2 sites, and the solid symbols are the measured proportion at different concentrations, Huang et al¹⁰. The inset shows the calculated contribution of sodium ordering to the heat capacity for $x=1/2$.

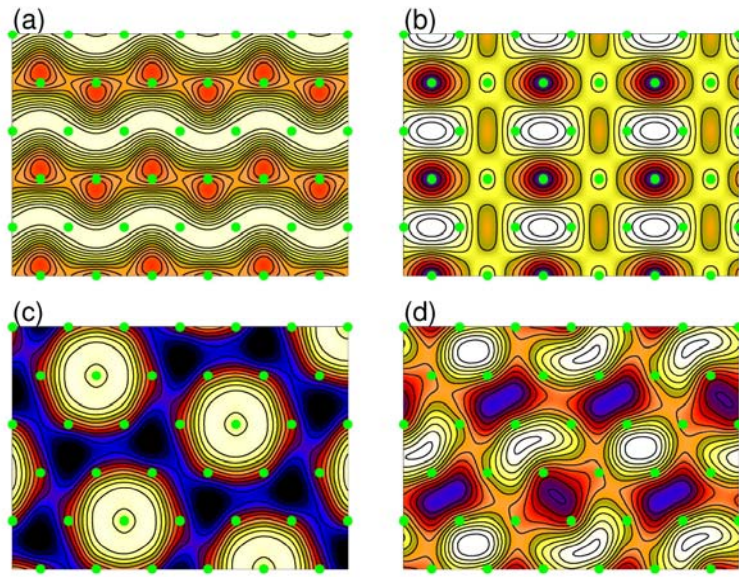


Figure 4: Coulomb potential in the Co plane calculated using ordered structures in Fig. 3. Positions of Co ions are shown as green circles. In-plane sodium structures are: (a) Divacancy array for $x=1/2$ with successive layers displaced by \mathbf{b}^{16} . The depth of the potential wells is of order 100 meV. Holes should localise along white stripes in Co planes. (b) Divacancy array for $x=1/2$ with successive layers undisplaced. (c) Divacancy array for $x=5/7$, aligned in the c direction, giving highest (hexagonal) symmetry. Each well carries two holes, one of them is localised at the minimum, and the other is delocalized on the surrounding hexagon. (d) Aligned trivacancy array for $x=3/4$. The number of potential wells is three times the number of Na trivacancies, and four Co sites at the periphery of each well share one hole.